

# Reaction Mechanism of the Metal Precursor Pulse in Atomic Layer Deposition of Ruthenium and Cobalt and the Role of Surface Facet NH/NH<sub>2</sub> Coverage

Ji Liu<sup>a</sup> and Michael Nolan<sup>a,\*</sup>

<sup>a</sup> Tyndall National Institute, University College Cork, Lee Maltings, Dyke Parade, Cork, T12 R5CP, Ireland

Corresponding author:

\*E-mail: Michael.nolan@tyndall.ie. Tel: +353 021 2346983

## Abstract

Ruthenium and Cobalt are potential candidate in replacing copper for interconnects and have been applied in the trenches and vias in semiconductor industry. A non-oxidizing reactant is required in atomic layer deposition (ALD) of thin films of these metals to avoid O-contamination. ALD of Ru and Co has been demonstrated experimentally, but the growth mechanism and key reactions are not clear. In this paper, the reaction mechanism of metal cyclopentadienyl (Cp, C<sub>5</sub>H<sub>5</sub>) precursors (RuCp<sub>2</sub> and CoCp<sub>2</sub>) and NH<sub>x</sub>-terminated metal surfaces (Ru and Co) is studied by density functional theory (DFT) calculations. The Cp ligands are eliminated by CpH formation via a hydrogen transfer step and may desorb from metal surface. The nature of the NH<sub>x</sub>-termination plays an important role in the reaction energies and barriers as does the surface facet on Ru and Co, with (001) and (100) surfaces showing different reaction energetics. The results show that on the NH<sub>x</sub>-terminated surfaces corresponding to ALD operating condition (temperature range 550K to 650K), the two Cp ligands can be eliminated completely on both Ru and Co (100) surface during the metal precursor pulse, resulting in Ru or Co atom deposited on the (100) surface. But the second Cp ligand reaction of hydrogen transfer is thermodynamically unfavourable on the (001) surface, resulting in RuCp or CoCp fragment termination on (001) surface, along with the possibility of surface bonded CpH. CoCp<sub>2</sub> always has lower reaction barriers than RuCp<sub>2</sub>, regardless of surface facets or NH<sub>x</sub> coverage. These final structures after metal precursor pulse are essential to model the reaction during the following N-plasma step.

## 1. Introduction

Copper (Cu) has been widely used in the semiconductor industry as interconnect for 20 years.<sup>1</sup> However, continuous deposition of Cu films needed for interconnect in nanoelectronics is difficult and a barrier layer is required to prevent the diffusion of Cu into the dielectric layer and Si substrates. Cu also aggregates into 3D structures.<sup>2-3</sup> Finding suitable barrier/liner layer is still a challenge because issues with copper reduce the electrical resistivity of the interconnect, especially for devices at nanosize dimension. One solution is to replace Cu with metals that do not suffer these issues. Transition metals Ruthenium (Ru) and Cobalt (Co) are important as candidates in replacing Cu for interconnects and have been applied in the trenches and vias with the downsizing of semiconductor devices.<sup>4-6</sup> In addition, Ru and Co are potential materials for the electrode in DRAM capacitors and MOSFETs.<sup>7</sup> There is also the question of deposition of nanoscale films, in particular on high aspect ratio structures, where different surface facets maybe present. Atomic layer deposition (ALD) is applied for conformal deposition and growth control at the atomic level, which is needed for deposition onto high aspect ratio structures.<sup>8-9</sup> Generally, ALD consists of two self-limiting half cycles, where the reactions will stop after all available surface sites are consumed. In addition to the successful application of ALD in microelectronics and the semiconductor industry, it is further applied in the areas of catalysis and energy conversion and storage.<sup>5, 10-11</sup>

The study of Ru ALD starts with precursors RuCp<sub>2</sub> and O<sub>2</sub>. The reported main byproducts are CO<sub>2</sub> and H<sub>2</sub>O.<sup>12</sup> For the thermal ALD growth, the reported growth rate is 0.45 Å/cycle with RuCp<sub>2</sub> and oxygen as the reactant.<sup>13</sup> By modifying the ligands, the properties of the metal precursor can be turned. For example, an ethyl group modification of Cp (Ru(EtCp)<sub>2</sub>) can lower the melting point.<sup>4</sup> Organometallic compounds such as β-diketonates have also been used in Ru precursors and the deposited Ru thin film has slightly higher level of impurity compared to metallocenes such as

RuCp<sub>2</sub>.<sup>14</sup> Since oxygen is involved in the deposition process, the quality of deposited Ru thin films depends strongly on oxygen dose.<sup>15-16</sup> Obviously, oxygen can result in formation of interfacial metal oxides, namely RuO<sub>2</sub>.<sup>15</sup> To address this problem, non-oxidizing reactants such as NH<sub>3</sub> can be applied to deposit metal thin films.<sup>17-19</sup> In addition to thermal ALD, plasma enhanced ALD (PE-ALD) has been developed with NH<sub>3</sub> or a mixture of N<sub>2</sub> and H<sub>2</sub> as the N-plasma source, which can be performed at temperature as low as 100°C.<sup>20</sup> For the PE-ALD of Ru using NH<sub>3</sub> plasma, the reported growth rate is 1.2 Å/cycle from metal precursor RuCp<sub>2</sub> and 1.8 Å/cycle from metal precursor Ru(EtCp)<sub>2</sub> at 300 °C.<sup>21</sup> The deposited Ru thin film is crystalline with hexagonal structure. The orientation is random at low temperature. However, the [001] direction will dominate at higher temperature or increased plasma power.<sup>4</sup> PE-ALD of Ru shows no nucleation delay and high plasma power is essential to obtain high quality Ru films.<sup>21</sup> One possible mechanism for PE-ALD is the presence of highly reactive radicals from NH<sub>3</sub>. But the detailed mechanism requires further study.

For the ALD of Co, Cp based precursors such as CoCp<sub>2</sub>, CoCp(CO)<sub>2</sub> and Co(CpAMD) have been developed and applied.<sup>22-23</sup> For thermal ALD of Co with metal precursor and hydrogen reactant, the required growth temperature can be as high as 350°C, but the growth rate is as low as 0.12 Å/cycle.<sup>24</sup> With the application of PE-ALD, the temperature can be reduced to 75°C. The reported growth cycle with CoCp<sub>2</sub> is increased to 1.5 Å/cycle, which is larger than that for RuCp<sub>2</sub>.<sup>25-26</sup> For the N-plasma source, a mixture of N<sub>2</sub> and H<sub>2</sub> is used and the properties of the deposited Co thin film greatly depend on the N<sub>2</sub>/H<sub>2</sub> gas flow ratio.<sup>27-28</sup> It is noted that H<sub>2</sub> plasma alone or individual N<sub>2</sub> and H<sub>2</sub> plasma results in high resistivity and low purity Co thin films. Previous studies argue that the presence of NH<sub>x</sub> species is needed to deposit low resistivity and high purity Co thin film.<sup>29</sup> NH<sub>x</sub> species are needed for chemisorption of metal precursor and removal of the Cp ligand. But

they are not incorporated in the film, because most of the N may desorb in the form of either  $\text{NH}_3$  or  $\text{N}_2$ . The detailed mechanism requires deeper study but one possible reason is that highly reactive radicals from N-plasma source should be present for successful PE-ALD of Co, which is similar to PE-ALD of Ru.

Density functional theory (DFT) calculations have been successfully applied to study the ALD of metals and metal oxides.<sup>30-33</sup> There are some outstanding questions, including how to design new precursors with properties such as good volatility and high reactivity or the mechanism of plasma enhanced ALD. Theoretically, the design and large-scale screening of precursors based on specific criteria such as the thermodynamic stability and kinetic stability have been performed in ALD modelling.<sup>34-35</sup> DFT calculations can also be applied to reveal the reaction mechanisms and the derived growth rate serves as guideline to experiments. In the early stage, the deposition of metal oxide, such as  $\text{Al}_2\text{O}_3$  from trimethylaluminum and  $\text{O}_3/\text{H}_2\text{O}$  as the co-reactant, has been studied theoretically.<sup>36-40</sup> The surface hydroxyl groups are formed and their surface coverages affect the growth rate. Additionally, other metal oxides such as  $\text{ZrO}_2$ ,  $\text{TiO}_2$ , and  $\text{HfO}_2$  have been investigated and reported.<sup>41-46</sup> For the deposition of metals, Elliott has proposed a mechanism for deposition of noble metals including Pd, Ir and Pt using homoleptic precursors and oxygen from DFT calculations.<sup>47</sup> It is found that each ligand is replaced by a hydroxyl group, which can be further eliminated by Brønsted-type reaction.

The reaction mechanism using oxidizing reactant such as  $\text{O}_3$  and  $\text{H}_2\text{O}$  is well-established. However, when depositing metals, O-source can promote oxidation of the metal surface and therefore cause contamination. Non-oxidizing reactants such as  $\text{NH}_3$  in PE-ALD of transition metals have been experimentally developed. A complete PE-ALD process using N-plasma is as follows. Firstly, it is vital to note that at the post-plasma stage, the metal surface is actually the

$\text{NH}_x$ -terminated metal surface. In the first half-cycle, the metal precursor ( $\text{RuCp}_2$  and  $\text{CoCp}_2$ ) reacts with  $\text{NH}_x$ -terminated metal surface. The Cp ligand is eliminated by proton transfer from the surface to form CpH, which desorbs from surface. In the second half-cycle, the plasma generated radicals such as  $\text{N}_x\text{H}_y$  will react with the precursor fragment terminated metal surface and the Ru or Co atoms are deposited on the surface, which is covered by  $\text{NH}_x$  groups at the end of second half cycle. In our recent published work, the nature and stability of  $\text{NH}_x$ -terminated metal surfaces were studied.<sup>48</sup> The results show that at ALD operating condition (temperature range 550K to 650K), on the low energy (001) surface, NH-termination at 1ML is the most stable surface termination, while on the high energy (100) surface, a mixture of NH and  $\text{NH}_2$  at 2ML is the most stable surface termination.

In this paper, we explore the reaction mechanism for the metal precursor pulse by DFT calculations. The metal precursor ( $\text{RuCp}_2$  or  $\text{CoCp}_2$ ) is adsorbed on the  $\text{NH}_x$ -terminated surfaces<sup>48</sup> and the hydrogen transfer step is studied in detail with calculation of proton migration barrier. After the first CpH formation and desorption, the possibility of the loss of second Cp ligand is also investigated. With the  $\text{NH}_x$  terminations at ALD operating condition, on the metal (100) surface, the metal precursor can undergo two hydrogen transfer steps and the two Cp ligands can be eliminated, resulting in metal atom deposition on the surface, binding to N atom. However, at most one Cp ligand can be eliminated on the metal (001) surface, resulting in  $\text{RuCp}$  or  $\text{CoCp}$  fragments on the surface after the metal precursor pulse, with possibility of surface-bonded CpH. During the next plasma step, the second Cp may be eliminated by highly reactive plasma radicals, which is the subject of ongoing work and beyond the scope of this paper. For the hydrogen transfer step,  $\text{CoCp}_2$  always has lower barriers than  $\text{RuCp}_2$ , regardless of surface facets and  $\text{NH}_x$  coverage. It is therefore concluded that the growth of Ru film is slower than Co film.

## 2. Methods and Computational Details

All the calculations are performed on the basis of spin-polarized DFT with the projector augmented wave (PAW) formalism<sup>49</sup>, as implemented in the Vienna *ab initio* simulations package (VASP 5.3) code. The generalized gradient approximation (GGA) with the parameterization of Perdrew-Burke-Ernzerhof (PBE) is used for the exchange-correlation functional.<sup>50-51</sup> The valence electrons are 9 for Co, 8 for Ru, 5 for N, 4 for C, and 1 for H. The energy cutoff is set to be 400eV for the plane wave expansion. The convergence of energy and forces are set to be  $1 \times 10^{-4}$  eV and  $0.01 \text{ eV}/\text{\AA}$ , respectively. The bulk Co and Ru crystal structure is optimized by simultaneously relaxing the ionic positions, cell volume and cell shape at a higher plane wave energy cutoff of 550eV and a Monkhorst-Pack grid k-point mesh<sup>52</sup> of  $12 \times 12 \times 6$ . The resulting lattice constants are  $a = b = 2.49 \text{\AA}$ , and  $c = 4.03 \text{\AA}$  for Co bulk and  $a = b = 2.71 \text{\AA}$ , and  $c = 4.28 \text{\AA}$  for Ru bulk.

The deposited Co or Ru films by ALD are polycrystalline and have random surface orientations after low temperature deposition. Based on our previous study<sup>48</sup> on the stability of NH/NH<sub>2</sub> terminations, we have chosen the most stable (001) surface and the least stable, and high reactivity surface, (100) to investigate on the precursor reaction mechanism. (001) surface has smaller surface area than (100) surface. Thus, a (4×4) supercell is used to simulate (001) surface while a (3×3) supercell is used to simulate (100) surface. The calculated surface area is  $1.18 \text{ nm}^2$  for Ru(001) and  $0.99 \text{ nm}^2$  for Co(001) with (4×4) supercell, while that for Ru(100) and Co(100) is  $0.99 \text{ nm}^2$  and  $0.90 \text{ nm}^2$  with (3×3) supercell. For (001) surface, a five-layer structure is built with the bottom three layer fixed during the calculation; while for (100) surface, due to unique zigzag structure, a four-bilayer (in total eight layers) structure is built with the bottom two bilayer (bottom four layers) fixed during the calculations. From our previous studies, fixing bottom three-layers is

sufficient to model these Ru and Co surfaces.<sup>48</sup> A k-point mesh<sup>52</sup> of  $2 \times 2 \times 1$  is used in (4×4) supercell and that for (3×3) supercell is  $3 \times 2 \times 1$ .

Our previous DFT study<sup>48</sup> of  $\text{NH}_x$  saturation coverage shows that at zero-K condition, the Ru(001) surface is terminated with 1ML NH and the Co(001) surface is terminated with 0.67ML NH and 0.23ML  $\text{NH}_2$ , which contains 10 NH and 4  $\text{NH}_2$  in (4×4) supercell. On (100) surfaces, the termination is 1ML NH and 1ML  $\text{NH}_2$  due to the trench structure, which contains 9 NH and 9  $\text{NH}_2$  in (3×3) supercell. The saturation coverages are summarized in Table 1. The configurations of the  $\text{NH}_x$ -terminated Ru and Co surfaces are shown in Figure 1(a)-(d).

Table 1. The calculated saturation coverages on (001) and (100) surfaces at zero-K and ALD conditions.

	(4×4)		(3×3)	
	Ru(001)	Co(001)	Ru(100)	Co(100)
Zero-K condition	1ML NH	0.67ML NH + 0.23ML $\text{NH}_2$	1ML NH + 1ML $\text{NH}_2$	1ML NH + 1ML $\text{NH}_2$
ALD condition	0.89ML NH	0.56ML NH	0.67ML NH + 0.67ML $\text{NH}_2$	0.67ML NH + 0.67ML $\text{NH}_2$

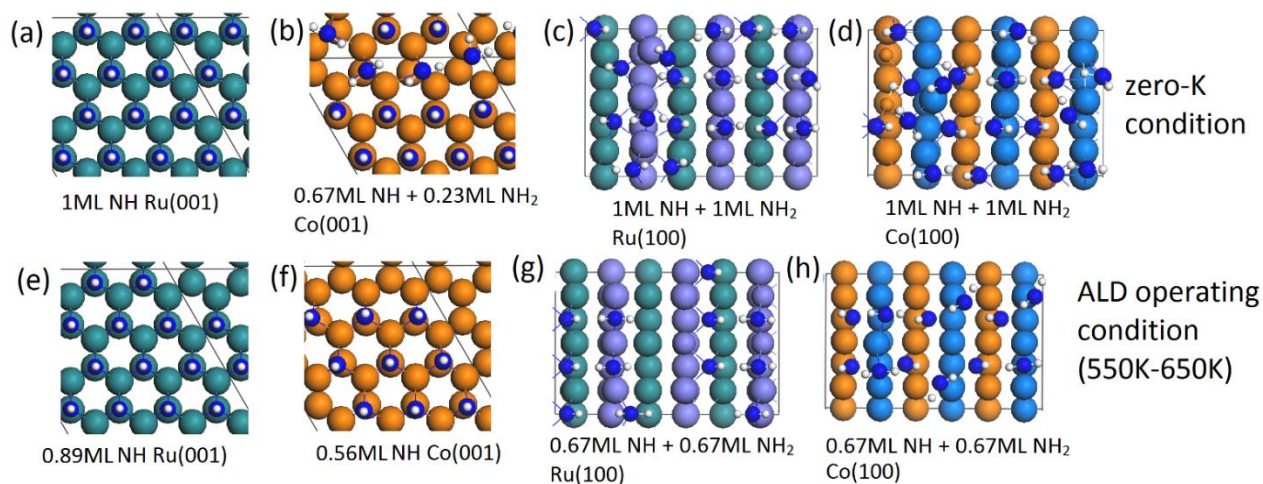


Figure 1. The top view of  $\text{NH}_x$  terminated metal surfaces at zero-K condition including (a) Ru(001), (b) Co(001), (c) Ru(100) and (d) Co(100) and at ALD operating condition including (e) Ru(001), (f) Co(001), (g) Ru(100) and (h) Co(100). Ru atom is represented by green and purple and Co atom is represented by orange and blue; N atom and H atom are represented by dark blue and white atom, respectively.

At ALD operating condition (temperature range 550K to 650K), some of the surface  $\text{NH}_x$  species desorb from the surface. The  $\text{NH}_x$  saturation coverage is as follows: Ru(001) surface is terminated with 0.89ML NH, which is 14 NH in (4×4) supercell and Co(001) surface is terminated with 0.56ML NH, which is 9 NH in (4×4) supercell. On the Ru and Co (100) surface, the preferred surface termination is 0.67ML NH and 0.67ML  $\text{NH}_2$ , which contains 6 NH and 6  $\text{NH}_2$  in (3×3) supercell. The configurations of  $\text{NH}_x$  terminations at the ALD operating condition are shown in Figure 1(e)-(h). On the (100) surface, due to the trench structure, NH prefers channel bridge site and  $\text{NH}_2$  prefers surface bridge site. Channel bridge is the bridge site with two channel metal atoms and surface bridge is the bridge site with two surface metal atoms. The configuration of single NH and  $\text{NH}_2$  adsorbed on channel bridge and surface bridge sites is shown in Figure S1 in the

supporting information. At zero-K condition, the saturation coverage is a full coverage of 1ML NH and 1ML NH<sub>2</sub>. At ALD operating condition, the saturation coverage is 0.67ML NH and 0.67ML NH<sub>2</sub>. However, the orientation depends on the metal. As shown in Figure 1(e)-(h), the orientation of NH and NH<sub>2</sub> is along y-direction on Ru(100) surface, while it is along x-direction on Co(100) surface.

The molecular geometries of the precursor RuCp<sub>2</sub> and CoCp<sub>2</sub> are individually relaxed in the same supercell as Ru(001) or Co(001), with the energy cutoff at 400eV and Gamma point sampling. The van der Waals correction is applied with PBE-D3 method to ensure an accurate description of the metal precursor adsorption energy.<sup>53</sup> The activation barriers reported in this paper are computed using climbing image nudged elastic band (CI-NEB) method<sup>54</sup> with 6 images including the starting and ending geometries and with the forces converged to 0.05eV/Å.

### 3. Results and Discussions

#### 3.1 Metal precursor adsorption on NH<sub>x</sub>-terminated (001) and (100) surfaces

The structure of free metal precursors is first addressed. For RuCp<sub>2</sub>, the Cp-Cp distance is 3.62Å and the Ru-C distance is 2.18Å. CoCp<sub>2</sub> has shorter Cp-Cp and Co-C distances. The Cp-Cp distance is between 3.39Å to 3.40Å. The Co-C distance is between 2.08Å to 2.10Å. This indicates some tilting of Cp rings of CoCp<sub>2</sub>.

When adsorbed on the NH<sub>x</sub> terminated metal surfaces, the metal precursor (RuCp<sub>2</sub> or CoCp<sub>2</sub>) can be placed perpendicular to substrate with one Cp ring interacting with the surface (the **upright** position) or parallel to surface with both Cp rings interacting with the surface (the **flat** position). The adsorption energy is calculated from:

$$E_{ad} = E_{tot} - \frac{E_{NH_x}}{Metal} - E_A \quad (1)$$

where  $E_{tot}$ ,  $E_{NH_x/Metal}$ , and  $E_A$  are the energy of the  $NH_x$ -terminated metal slab with precursor A ( $A = RuCp_2, CoCp_2$ ), the slab model for the  $NH_x$ -terminated metal surface, and isolated precursor A ( $A = RuCp_2, CoCp_2$ ), respectively. All the energies are computed with van der Waals correction. A negative adsorption energy corresponds to exothermic adsorption.

### 3.1.1 Metal precursor adsorption on $NH_x$ -terminated (001) and (100) surfaces at zero-K condition

The calculated adsorption energies of the metal precursors on  $NH_x$ -terminated (001) and (100) surfaces corresponding to the zero-K condition are shown in Table 2. On the (001) surface, the metal precursor prefers to bind to the substrate in the upright adsorption mode through only one Cp ring. On the (100) surface, the metal precursor prefers to bind to the substrate through both Cp rings with the precursor in the flat configuration. These structures are shown in Figure 2. The configurations of less stable adsorption structures are shown in Figure S2 of supporting information.

This difference in binding mode at the two surface facets is due to the different surface structures. The (001) surface has a flat surface structure, while (100) surface has a unique zigzag structure. On the (001) surface, an upright position with one Cp ring close to metal surface can result in stronger adsorption strength. With this upright binding mode, each carbon atom in the Cp ring is available for the hydrogen transfer step to form CpH. The distances between the two Cp rings are in the range of 3.62Å to 3.65Å for  $RuCp_2$  on Ru(001) surface and 3.38Å to 3.43Å for  $CoCp_2$  on Co(001) surface. The distances for metal-C are 2.17Å to 2.19Å for  $RuCp_2$  and between 2.08Å and 2.11Å for  $CoCp_2$ . Compared to free metal Cp precursors, the distances between the two Cp rings are enlarged for  $RuCp_2$  and  $CoCp_2$ .

Table 2. The calculated adsorption energy of metal precursor RuCp<sub>2</sub> and CoCp<sub>2</sub> adsorbed on (001) and (100) surfaces. The NH/NH<sub>2</sub> terminations correspond to the zero-K condition.

	(001)		(100)	
	RuCp <sub>2</sub> /eV	CoCp <sub>2</sub> /eV	RuCp <sub>2</sub> /eV	CoCp <sub>2</sub> /eV
<b>upright</b>	-1.47	-0.10	-0.77	-1.41
<b>flat</b>	-1.28	3.16	-1.89	-1.73

On the (100) surface, the distances across the trench (between two neighbouring metal atoms) are 4.29Å on Ru(100) surface and 4.03Å on Co(100) surface. The distances between the two Cp rings in precursors are in the range of 3.56Å to 3.68Å for RuCp<sub>2</sub> on Ru(100) surface and 3.34Å to 3.44Å for CoCp<sub>2</sub> on Co(100) surface. The distances for metal-C are 2.18Å to 2.19Å for RuCp<sub>2</sub> and 2.07Å to 2.10Å for CoCp<sub>2</sub>. The metal precursor can be well-accommodated within the trench of (100) surface, which promotes the adsorption of the precursor. With this flat binding mode, the carbon atom in the bottom of the Cp ring is available for perform hydrogen transfer to form CpH. Compared to free metal Cp precursors, the two Cp rings are tilted with shorter ring-ring distance for the atoms away from the surface and longer ring-ring distance for the atoms closer to the surface.

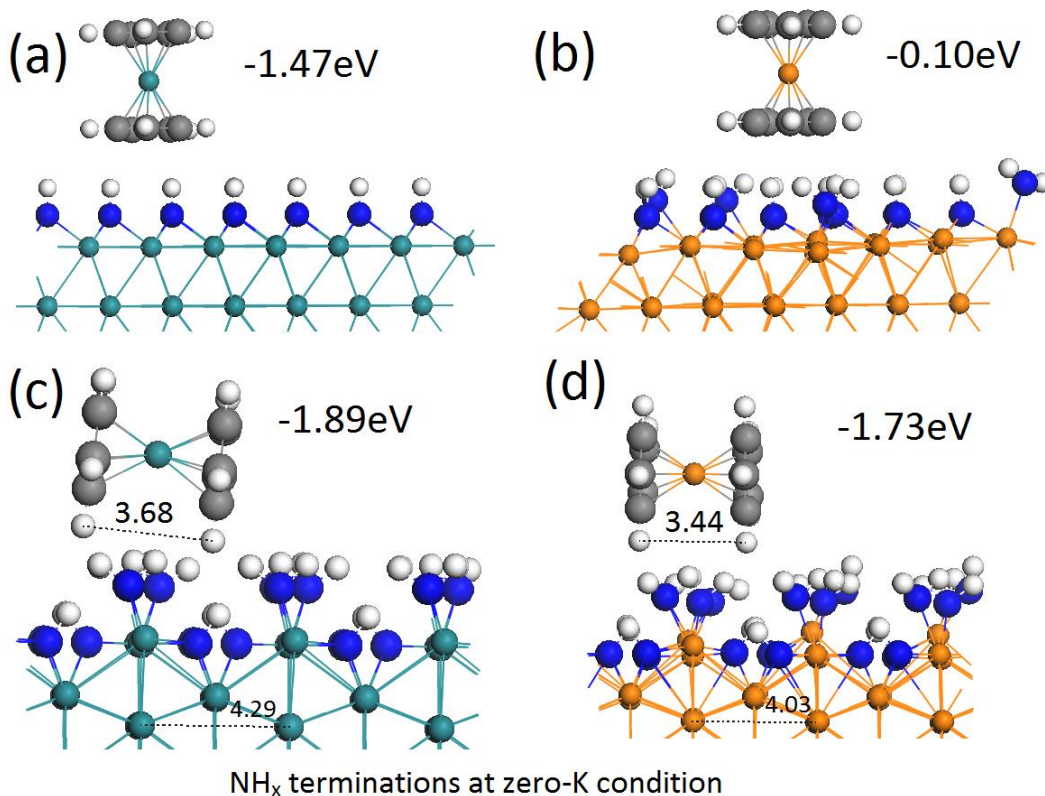


Figure 2. The configurations of the most stable adsorption of precursor RuCp<sub>2</sub> and CoCp<sub>2</sub> on (a) Ru(001) surface, (b) Co(001) surface, (c) Ru(100) surface, and (d) Co(100) surface. The NH<sub>x</sub> termination is with respect to zero-K condition. Ru atom is represented by green and Co atom is represented by orange; N atom and H atom are represented by dark blue and white atom, respectively.

### 3.1.2 Metal precursor adsorption on NH<sub>x</sub>-terminated (001) and (100) surfaces at ALD operating condition

The calculated adsorption energy of the metal precursors on the NH<sub>x</sub>-terminated (001) and (100) surfaces corresponding to ALD operating condition are shown in Table 3. With increased temperature, the NH<sub>x</sub> terminations have changed. On (001) surface, Ru(001) is terminated with

Table 3. The calculated adsorption energy of metal precursor RuCp<sub>2</sub> and CoCp<sub>2</sub> adsorbed on (001) and (100) surfaces. The NH/NH<sub>2</sub> terminations corresponds to ALD operating condition (temperature range 550K - 650K).

	(001)		(100)	
	RuCp <sub>2</sub> /eV	CoCp <sub>2</sub> /eV	RuCp <sub>2</sub> /eV	CoCp <sub>2</sub> /eV
<b>upright</b>	-1.47	-0.68	-0.57	-0.34
<b>flat</b>	-0.61	-0.56	-0.75	-1.67

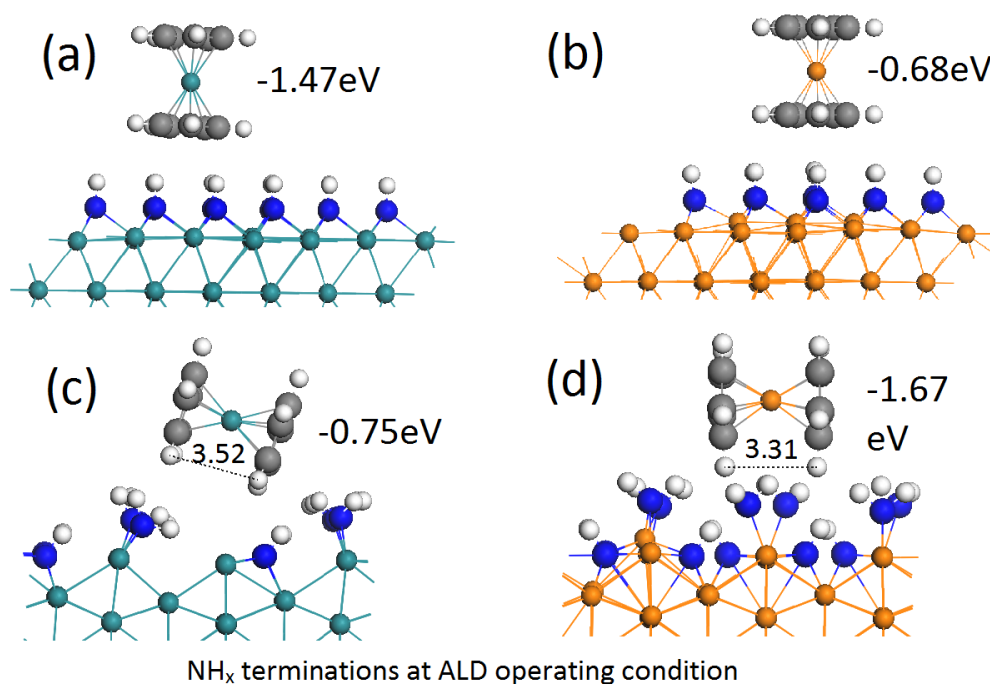


Figure 3. The configurations of the most stable adsorption of precursor RuCp<sub>2</sub> and CoCp<sub>2</sub> on (a) Ru(001) surface, (b) Co(001) surface, (c) Ru(100) surface, and (d) Co(100) surface. The NH<sub>x</sub> termination is with respect to ALD operating condition. Ru atom is represented by green and Co atom is represented by orange; N atom and H atom are represented by dark blue and white atom, respectively.

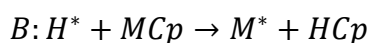
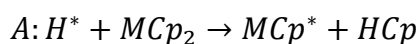
0.89ML NH and Co(001) is terminated with 0.56ML NH; on both Ru(100) and Co(100) surfaces, the termination is mixed termination with 0.67ML NH and 0.67ML NH<sub>2</sub>.

For both precursors and surfaces, the binding preference of metal precursor is the same as the zero-K terminated surfaces. These structures are shown in Figure 3. The configurations of less stable adsorption structures are shown in Figure S3 of supporting information. On the (001) surface, an upright position with one Cp ring close to metal surface can result in stronger adsorption strength (lower adsorption energy). The distances between the two Cp rings are in the range of 3.59Å to 3.64Å for RuCp<sub>2</sub> on Ru(001) surface and 3.37Å to 3.40Å for CoCp<sub>2</sub> on Co(001) surface. Compared with free RuCp<sub>2</sub> or CoCp<sub>2</sub>, the two Cp rings are slightly tilted. The distances for metal-C are between 2.17Å and 2.20Å of RuCp<sub>2</sub> and between 2.08Å and 2.10Å of CoCp<sub>2</sub>.

On (100) surface, the distances of the trench (two neighbouring metal atoms) are 4.29Å on Ru(100) surface and 4.03Å on Co(100) surface. The distances between the two Cp rings are in the range of 3.52Å to 3.69Å for RuCp<sub>2</sub> on Ru(100) surface and 3.31Å to 3.40Å for CoCp<sub>2</sub> on Co(100) surface. The distances for metal-C are 2.19Å to 2.20Å for RuCp<sub>2</sub> and 2.06Å to 2.10Å for CoCp<sub>2</sub>. The flat adsorption mode of metal precursor can be well-accommodated within the trench of the (100) surfaces, which can result in stronger adsorption strength. Compared to free metal Cp precursors, the two Cp rings are tilted with shorter ring-ring distances for the atoms closer to the surface and longer ring-ring distances for the atoms away from the surface. This is different from the adsorption mode at the zero-K condition, where shorter ring-ring distance is for the atoms away from the surface and the longer ring-ring distance is for the atoms closer to the surface.

*3.2 Precursor reaction mechanism on (001) and (100) surfaces with NH<sub>x</sub> terminations at zero-K condition*

We have first addressed the reaction mechanism with respect to the NH<sub>x</sub> terminations at zero-K condition. These terminations are 1ML NH on Ru(001) surface, 0.67ML NH and 0.23ML NH<sub>2</sub> on Co(001) surface, and 1ML NH and 1ML NH<sub>2</sub> on Ru and Co (100) surfaces. Once the metal precursor is adsorbed on NH<sub>x</sub>-terminated metal surfaces, the Cp ligand can undergo hydrogen transfer, CpH formation, CpH desorption, second hydrogen transfer, and second CpH formation and desorption. Upon adsorption, no spontaneous hydrogen transfer was observed on all Ru and Co (001) and (100) surfaces. This means that the hydrogen transfer step must overcome an activation barrier. The reaction of a single precursor molecule of MCp<sub>2</sub> (M = Ru, Co) on the NH<sub>x</sub> terminated metal surface can be illustrated as follows:



where reaction A involves the first Cp ligand and reaction B involves the second Cp ligand. We have calculated the energy along the reaction pathway and the activation barriers for hydrogen transfer steps during the reaction. The results are summarized in Figure 4 and Figure 5 for (001) and (100) surfaces of Ru and Co. The calculated barriers for the hydrogen transfer steps are presented in Table 4. The configurations of the corresponding transition states are shown in Figure S4-S9 of the supporting information. For the second H transfer to Cp, if the computed reaction energy with reference to the NH<sub>x</sub>-terminated metal surface and isolated MCp<sub>2</sub> (M=Ru, Co) is positive, then the barrier for the second hydrogen transfer step is not calculated. The positive reaction energy implies that the surface will be terminated with the MCp fragment at the end of metal pulse.

The reaction energies of precursor adsorption ( $E_{\text{adsorption}}$ ), first hydrogen transfer ( $E_{\text{hydrogen}}^{\text{I}}$ ), and first CpH formation ( $E_{\text{CpHformation}}^{\text{I}}$ ) are with reference to the  $\text{NH}_x$ -terminated metal surface and free  $\text{MCp}_2$ . If one CpH molecule desorbs from the surface, the reaction energies of first CpH desorption ( $E_{\text{CpHdesorption}}^{\text{I}}$ ), second hydrogen transfer ( $E_{\text{hydrogen}}^{\text{II}}$ ), and second CpH desorption ( $E_{\text{CpHdesorption}}^{\text{II}}$ ) are with reference to  $\text{NH}_x$ -terminated metal surface, free  $\text{MCp}_2$ , and free CpH.

Table 4. The calculated reaction energy for hydrogen transfer step and reaction barriers on (001) and (100) surfaces with  $\text{NH}_x$  terminations corresponding to zero-K condition in eV. If the reaction energy is positive, the barrier for the next hydrogen transfer step is not calculated. For Ru(001), the second hydrogen transfer is achievable with the presence of surface CpH.

	$H^* + \text{MCp}_2 \rightarrow \text{MCp}^* + \text{HCp}$			$H^* + \text{MCp} \rightarrow M^* + \text{HCp}$		
	$E_{\text{adsorption}}$	$E_{\text{hydrogen}}^{\text{I}}$	$E_{\text{barrier}}$	$E_{\text{CpHdesorption}}^{\text{I}}$	$E_{\text{hydrogen}}^{\text{II}}$	$E_{\text{barrier}}$
Ru(001)	-1.47	-0.17	1.33	-0.34 (CpH adsorbed)	-0.04 (CpH adsorbed)	0.98 (CpH adsorbed)
Co(001)	-0.10	-0.76	1.00	-2.34	-2.46	1.24
Ru(100)	-1.94	-0.79	2.72	1.92	1.19	Not Calculated
Co(100)	-1.73	-3.12	1.56	-1.17	-1.72	0.84

On the Ru(001) surface, after adsorbing on  $\text{NH}_x$ -terminated metal surface,  $\text{RuCp}_2$  has a stronger adsorption strength (-1.47eV) than  $\text{CoCp}_2$  (-0.10eV). For the hydrogen transfer step, the reaction energy difference ( $\Delta E$ ) on the Ru(001) surface is positive (1.30eV) with a high proton transfer barrier of 1.33eV. On the Co(001) surface, the reaction energy difference is negative (-0.66eV) with a computed barrier of 1.00eV. This means that the hydrogen transfer step is endothermic on

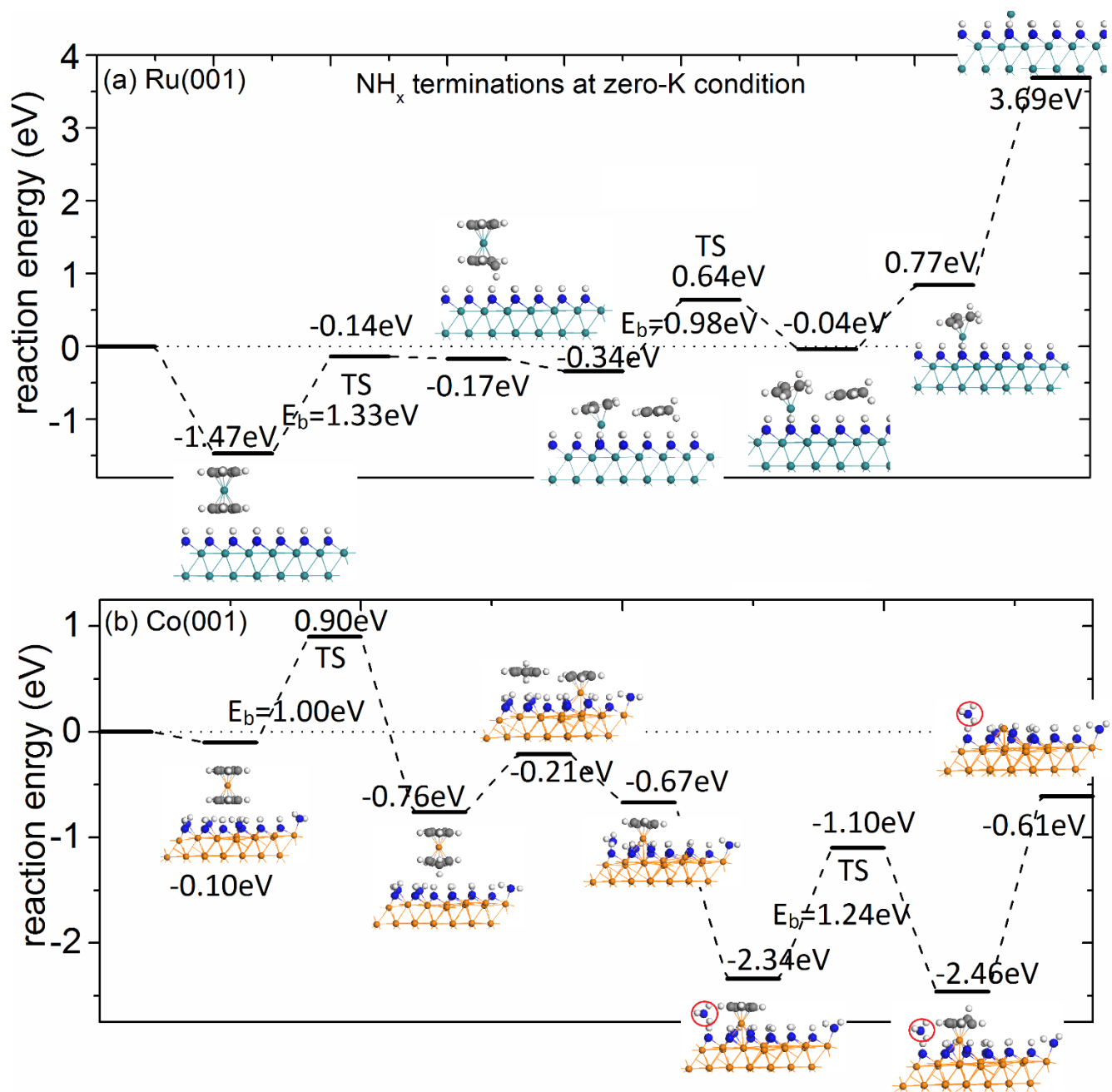


Figure 4. The plotted metal precursor reaction pathway on (a) Ru(001) surface and (b) Co(001) with  $\text{NH}_x$  terminations at zero-K condition. On Ru(001) surface, the reaction will stop after the second hydrogen transfer. On Co(001) surface, both of the Cp ligands can be eliminated with Co atoms deposited on the surface.

Ru(001) surface with a high barrier but it is exothermic on Co(001) surface with a moderate barrier. The overall reaction for  $\text{MCp}_2$  (M=Ru or Co) adsorption and CpH formation is exothermic on Ru(001) and Co(001) surfaces. However, as shown in Figure S10 in the supporting information, after the CpH formation on Ru(001), the desorption of CpH is endothermic with a positive reaction energy difference of 0.80eV. In addition, the energies on Ru(001) are clearly unfavourable along the pathway for the second CpH formation and desorption. After the second Cp ligand desorption, the reaction energy is as high as 3.69eV. Since the desorption of CpH is endothermic, we have calculated the second hydrogen transfer with presence of CpH and the results are shown in Figure 4(a). The second hydrogen transfer step is slightly endothermic with a positive reaction energy difference of 0.30eV and a moderate barrier of 0.98eV. This implies that with CpH adsorbed on the surface, the second hydrogen transfer is achievable on the Ru(001) surface. The final termination is the Ru atom and two surface CpH molecules. One CpH molecule is bonded to Ru atom and the other one is bonded to NH species.

By contrast, the desorption of first CpH is exothermic on Co(001) surface. After the first Cp ligand desorbs from the surface exothermically, the CoCp fragment (Co atom and the remaining Cp ring) is adsorbed on the surface with Co atom binding to the N atom, from which the proton has transferred. At the same time, the surface  $\text{NH}_x$  termination has changed, and one  $\text{NH}_3$  molecule is formed. This  $\text{NH}_3$  can desorb easily from the surface. Surface terminating N and H species may be eliminated via  $\text{NH}_3$  formation during the metal precursor step as well as during the next plasma step to deposit metal atom onto the surface. The second hydrogen transfer is slightly exothermic with negative reaction energy difference of -0.12eV and has a moderate barrier of 1.24eV. Finally, after the second Cp ligand desorbs from surface as CpH, which is overall exothermic, the final adsorbate is Co atom binding to N atom that has lost H atom.

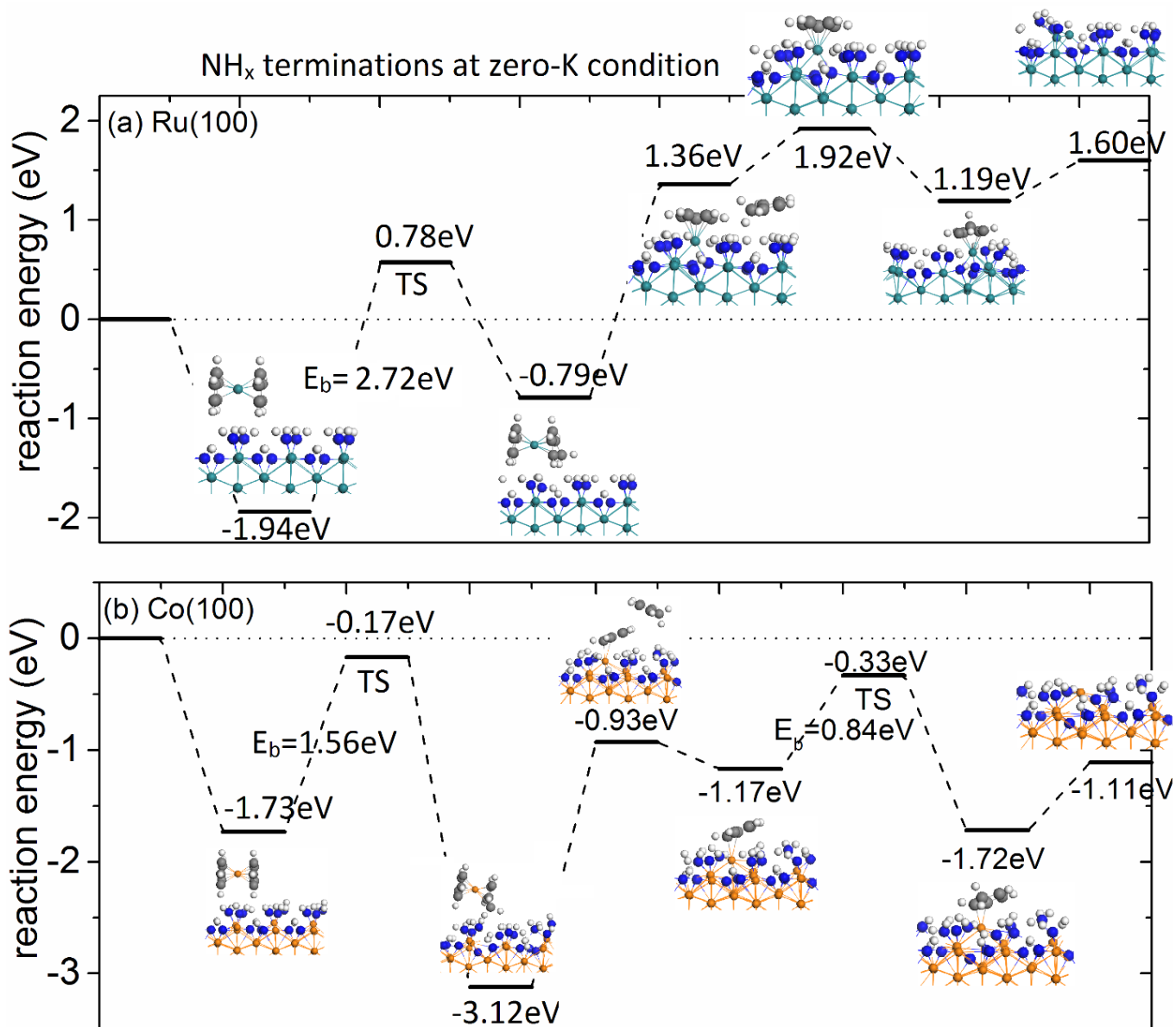


Figure 5. The plotted metal precursor reaction pathway on (a) Ru(100) surface and (b) Co(100) surface with  $\text{NH}_x$  terminations at zero-K condition. On Ru(100) surface, the reaction will stop after hydrogen transfer; and on Co(100) surface, both of the Cp ligands can be eliminated with Co atom deposited on the surface.

On the Ru(100) surface, at zero-K condition, the  $\text{NH}_x$  termination is  $9\text{NH}$  and  $9\text{NH}_2$ .  $\text{RuCp}_2$  and  $\text{CoCp}_2$  have significantly exothermic adsorption modes. For  $\text{RuCp}_2$ , the adsorption energy is  $-1.94\text{eV}$ , and that for  $\text{CoCp}_2$  is  $-1.73\text{eV}$ . During the hydrogen transfer step, H atom from channel NH is more reactive than H atom from surface  $\text{NH}_2$ . The results for transfer of different H species are summarized in Table 5. On the Ru(100) surface, the hydrogen transfer step from surface H is highly endothermic with a positive reaction energy difference of  $1.89\text{eV}$  at zero-K condition, while channel H is more favourable with a positive reaction energy difference of  $1.15\text{eV}$ . On the Co(100) surface, after structure relaxing, the surface N atom that has lost H atom can grab a H atom from the channel N and recover to  $\text{NH}_2$ .

Table 5. The calculated reaction energy for hydrogen transfer step from surface H and channel H on Ru(100) and Co(100) surfaces. The results for transfer of different H species show that channel H is more reactive than surface H on the metal (100) surfaces.

	Zero-K condition		ALD condition	
	Ru(100)/eV	Co(100)/eV	Ru(100)/eV	Co(100)/eV
adsorption	-1.94	-1.73	-2.85	-1.67
hydrogen transfer channel H	-0.79	-3.12	-1.44	-2.19
hydrogen transfer surface H	-0.05	Recover to $\text{NH}_2$	Recover to $\text{NH}_2$	Recover to $\text{NH}_2$

Thus, in the discussion of hydrogen transfer on (100) surfaces, channel H is the most active species for hydrogen transfer to the Cp ligand. For the hydrogen transfer step, the reaction energy difference ( $\Delta E$ ) on Ru(100) surface is positive (1.15eV) with a computed barrier as high as 2.72eV, while that on Co(100) surface is negative (-1.39eV) with a more moderate barrier of 1.56eV. This means that the hydrogen transfer step is endothermic on Ru(100) surface but it is exothermic on Co(100) surface. After the hydrogen transfer step, the CpH formation on Ru(100) surface is highly endothermic with a positive reaction energy difference of 2.15eV. This implies that on Ru(100) surface, the reaction will stop after hydrogen transfer step. The breaking of Ru-C bond to form CpH is extremely difficult. This may be achievable during the plasma step with the presence of highly reactive plasma radical that reacts with CpH.

By contrast, Co(100) shows higher reactivity and the second Cp reaction and desorption are favourable. After desorption of the first Cp ligand, the adsorbed CoCp will continue reacting through transfer of another channel H atom with an energy gain of -0.55eV and a moderate activation barrier of 0.84eV, which is exothermic. At this point, NH<sub>3</sub> is formed and can easily desorb from surface. Thus, each adsorbed CoCp<sub>2</sub> can undergo two hydrogen transfer steps and the two Cp ligands can desorb as CpH, which results in the Co atom binding to the N atom that has lost a proton.

With NH<sub>x</sub> termination at zero-K condition, on both (001) and (100) surfaces, CoCp<sub>2</sub> shows higher reactivity than RuCp<sub>2</sub>. The hydrogen step is the key step for Cp ligand elimination. The first hydrogen transfer step is endothermic on Ru(001). With the presence of CpH, the second hydrogen transfer is achievable, although the reaction is endothermic and has a moderate barrier, resulting Ru atom binding to N atom and two CpH molecules. One CpH molecule is bonded to Ru atom and the other one is bonded to surface NH species. On Ru(100) surface, the reaction will stop after first

hydrogen transfer step due to endothermic reaction of CpH formation. However, the hydrogen transfer step is exothermic on Co(001) and Co(100) surface and the two Cp ligands can be eliminated during the metal pulse, resulting in Co atom deposited on the surface. The final structures after single metal precursor  $MCp_2$  ( $M=Ru$  or  $Co$ ) adsorbing and reacting on  $NH_x$ -terminated metal (001) surfaces are shown in Figure 6.

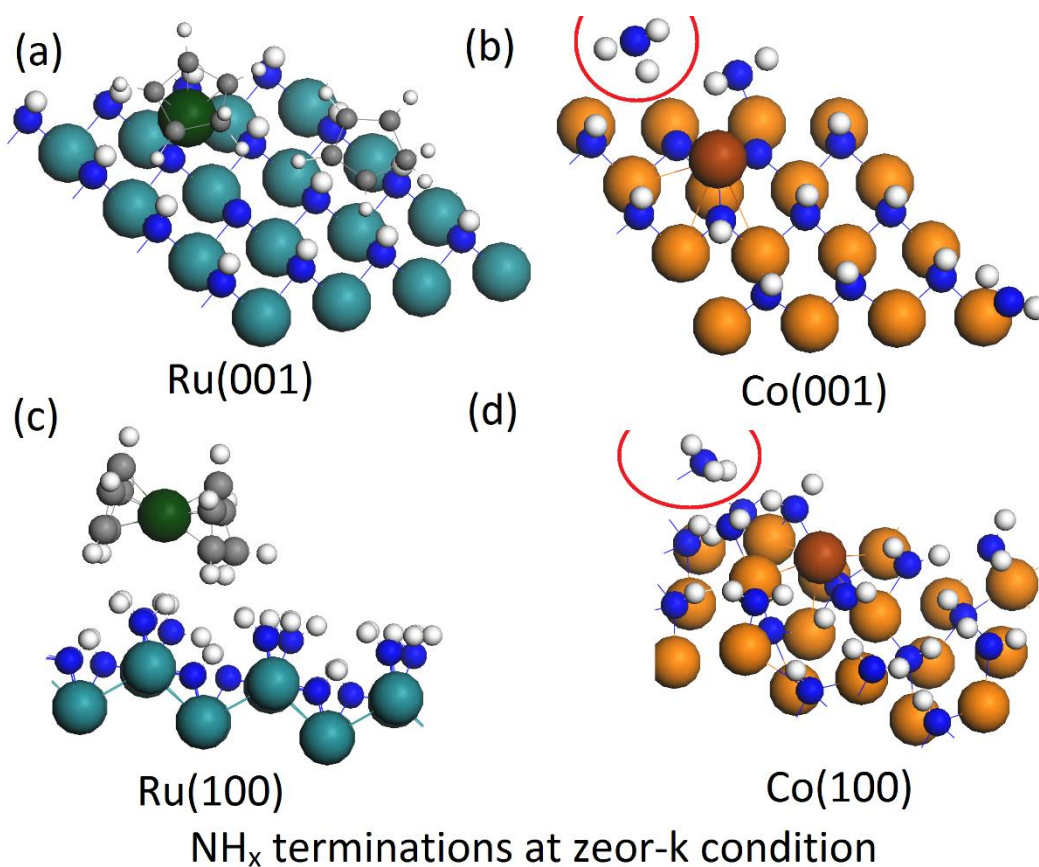


Figure 6. The configurations of the final structures after single metal precursor  $MCp_2$  ( $M=Ru$  or  $Co$ ) adsorption and ligand elimination on the (a) Ru(001), (b) Co(001), (c) Ru(100), and (d) Co(100) surface. The  $NH_x$  terminations are at zero-K condition.

3.3 Precursor reaction mechanism on (001) and (100) surfaces with NH<sub>x</sub> terminations at ALD operating condition

The coverage and nature of the NH<sub>x</sub> termination on the Ru and Co surfaces is expected to influence both the precursor adsorption strength and barriers and energetics of the hydrogen transfer and CpH removal steps. Our previous thermodynamic study<sup>48</sup> showed that at typical ALD operating conditions (temperature range 550K to 650K, 1.5 mTorr), the most favourable NH<sub>x</sub>-termination on the (001) surface is 14NH on Ru(001) and 9NH on Co(001). On the (100) surfaces, the most favourable terminations are 6NH and 6NH<sub>2</sub> on Ru(100) and Co(100).

Table 6. The calculated reaction energy for hydrogen transfer step and reaction barriers on (001) and (100) surfaces with NH<sub>x</sub> terminations corresponding to ALD operating condition. If the reaction energy is positive, the barrier for that hydrogen transfer step is not calculated.

	$H^* + MCp_2 \rightarrow MCp^* + HCp$			$H^* + MCp \rightarrow M^* + HCp$		
	E <sub>adsorption</sub>	E <sub>hydrogen</sub> <sup>I</sup>	E <sub>barrier</sub>	E <sub>CpH desorption</sub> <sup>I</sup>	E <sub>hydrogen</sub> <sup>II</sup>	E <sub>barrier</sub>
Ru(001)	-1.47	0.03	1.51	0.71	1.44	Not Calculated
Co(001)	-0.68	-0.36	0.40	0.12	0.91	Not Calculated
Ru(100)	-2.85	-1.44	2.01	-2.14	-1.68	1.00
Co(100)	-1.67	-2.19	0.52	-1.32	-1.15	0.85

With these coverages, we calculate the reaction energy along the reaction pathway discussed in Section 3.2 and the associated activation barriers for the hydrogen transfer steps during the reaction of the metal precursors with the most favourable NH<sub>x</sub> terminations at ALD operating conditions.

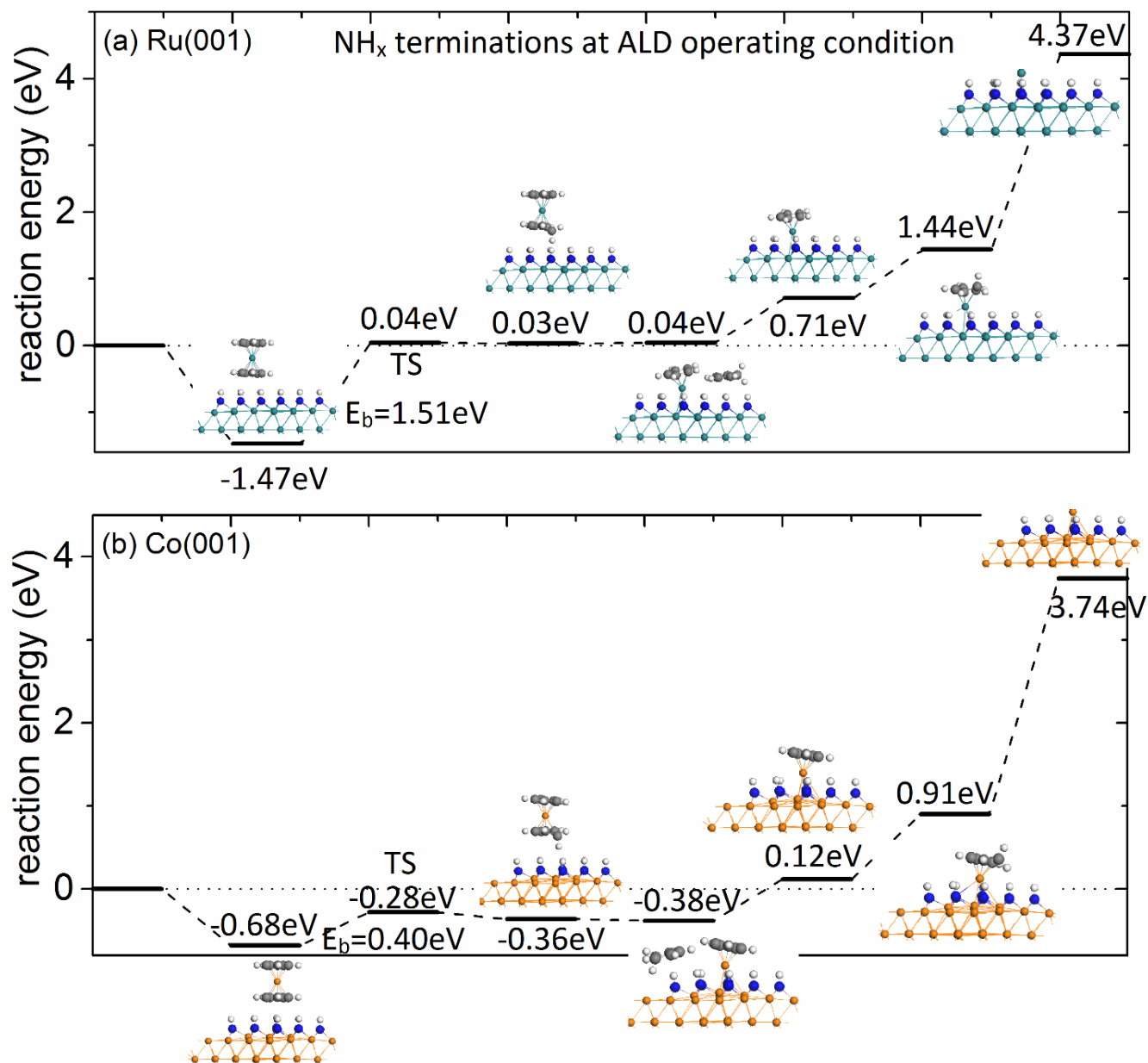


Figure 7. The plotted metal precursor reaction pathway on (a) Ru(001) surface and (b) Co(001) surface with  $\text{NH}_x$  terminations at ALD operating condition. On both Ru(001) and Co(001) surfaces, the reaction will stop after the first hydrogen transfer step.

The results of this analysis are summarized in Figure 7 and Figure 8 for the metal (001) and (100) surfaces. The computed barriers for the hydrogen transfer steps are listed in Table 6. The configurations of transition states are shown in Figure S11-S16 of supporting document.

At the Ru(001) surface, RuCp<sub>2</sub> has a strong adsorption energy of -1.47eV. With increased temperature, the surface termination is slightly reduced from 1ML at 0K termination to 0.89ML at typical ALD operating conditions. The adsorption strength of metal precursor RuCp<sub>2</sub> does not change. Similar to the 0K termination, after the first hydrogen transfer and CpH release, the reaction energies become endothermic. The first hydrogen transfer step has a high barrier of 1.51eV and is overall thermoneutral. The first CpH desorption leaving a RuCp surface termination is endothermic by 0.71eV. Computing the energy for the second CpH formation and desorption, we see that the reaction energy is as high as 4.37eV. Therefore, the final termination after introduction of the RuCp<sub>2</sub> precursor is a RuCp terminated surface, assuming that the initial activation barrier for the first hydrogen transfer can be overcome. The CpH may desorb from the surface at the ALD operating temperature, but its persisting on the surface needs to be considered.

On the Co(001) surface, the metal precursor CoCp<sub>2</sub> has a moderate adsorption energy of -0.68eV. The first hydrogen transfer step has a low barrier of 0.40eV, particularly when compared to that of the corresponding Ru(001) surface and the overall reaction is still exothermic by 0.36eV. After the first Cp ligand is eliminated, the second Cp cannot be eliminated due to an endothermic reaction energy. The final energy after the second CpH desorption is as high as 3.74eV. The overall reaction is exothermic for the first Cp ligand elimination so that the final termination will be a surface terminated with CoCp fragments. The desorption of CpH is slightly endothermic with positive reaction energy difference of 0.50eV. But the CpH should desorb from the surface at the ALD operating temperature.

At higher temperatures, the surface NH saturation coverage will be further reduced.<sup>48</sup> To examine this, we have calculated the reaction energy difference ( $\Delta E$ ) for the hydrogen transfer step at different NH coverages on Ru and Co (001)  $\text{NH}_x$  terminated surfaces and these are summarized in Table 7. On the Ru(001) surface, the zero-K surface termination is 1ML NH. If the temperature is increased to ALD operating condition (temperature range 550K to 650K), the surface termination will be reduced to 0.88ML NH. Now, we continue decreasing the coverage and set the surface termination of Ru(001) at 0.50ML NH, 0.25ML NH and 0.06ML NH. As listed in Table 7, the calculated reaction energy still remains positive for all coverages studied, and we can infer a high barrier for the hydrogen transfer step irrespective of the coverage of the NH surface termination. Thus, a single  $\text{RuCp}_2$  precursor has a high hydrogen transfer barrier on the Ru(001) surface and therefore, at most only one Cp ligand can be eliminated while the nature of the  $\text{NH}_x$ -termination has little effect on the elimination of the Cp ligand on Ru(001) surface.  $\text{RuCp}_2$  has been commonly used as Ru ALD precursor experimentally. For the thermal ALD growth, the reported growth rate is 0.45 Å/cycle with  $\text{RuCp}_2$  and oxygen as the reactant.<sup>13</sup> PE-ALD can significantly reduce the incubation.<sup>20</sup> The most commonly used precursor for PE-ALD of Ru is  $\text{Ru}(\text{EtCp})_2$ . The reported growth rate varies from 0.16 Å/cycle to 0.80 Å/cycle, depending on the process condition such as reactor temperature and pressure and plasma conditions.<sup>20</sup>

On the Co(001) surface, at zero-K, the surface termination is 0.67ML NH and 0.23ML  $\text{NH}_2$ . If the temperature increases to the ALD operating condition, the surface termination will be reduced to 0.56ML NH. Similar to Ru(001), we continue decreasing the coverage and set the surface termination to be 0.50ML NH, 0.25ML NH and 0.06ML NH. The calculated  $\Delta E$  depends on the  $\text{NH}_x$ -terminations. At lowest coverage, the energy of the hydrogen transfer step is endothermic but it becomes more favourable as the coverage increases, particularly for the highest coverage of

NH/NH<sub>2</sub>. The computed hydrogen transfer barriers on the Co(001) surface are low. For example, the computed activation barrier decreases from 1eV (for 0 K termination) to 0.40eV for the stable termination under ALD operating conditions. The nature of NH<sub>x</sub>-termination therefore plays an important role in the elimination of the Cp ligand on the Co(001) surface. The reported growth rate of PE-ALD of Co using CoCp<sub>2</sub> and N-plasma varies from 0.26 Å/cycle to 0.97 Å/cycle.<sup>25, 28-29</sup>, which would be consistent with the more favourable activation barriers and reaction energies computed for Co(001) over Ru(001).

Table 7. The calculated reaction energy difference ( $\Delta E$ ) hydrogen transfer step on Ru(001) and Co(001) surface with various NH<sub>x</sub>-terminations.  $\Delta E$  is calculated by the formula  $\Delta E = E_{\text{hydrogen}}^I - E_{\text{adsorption}}$ .

Ru(001)		ALD Temperature			Zero-K
	0.06ML NH	0.25ML NH	0.50ML NH	0.88ML NH	1ML NH
$\Delta E/eV$	1.51	1.68	1.69	1.50	1.30
Co(001)		ALD Temperature			Zero-K
	0.06ML NH	0.25ML NH	0.50ML NH	0.56ML NH	0.67ML NH + 0.23ML NH <sub>2</sub>
$\Delta E/eV$	0.60	0.30	0.15	0.32	-0.66
Barrier/eV	Not calculated	Not calculated	0.29	0.40	1.00

On the metal (100) surfaces, we find that for the hydrogen transfer step, channel H atom is more reactive than surface H atom. As listed in Table 5 in Section 3.2, if the hydrogen transfer is from H atom of surface NH<sub>2</sub>, after structure relaxing, surface N will grab the H atom from channel NH

and recover to surface  $\text{NH}_2$ . Thus, in the discussion on (100) surface, the channel H atom contributes to the hydrogen transfer.

On both Ru(100) and Co(100) surfaces under ALD conditions, the favourable  $\text{NH}_x$ -termination is  $6\text{NH}$  and  $6\text{NH}_2$ . On this Ru(100) surface,  $\text{RuCp}_2$  initially has a moderate exothermic adsorption energy,  $-0.74\text{eV}$  upon adsorption. After adsorption, before the hydrogen transfer step, the channel NH migrates to the surface NH site, which can greatly enhance the adsorption strength, giving a computed adsorption energy of  $-2.85\text{eV}$ . However, this does not mean that surface H atom from surface  $\text{NH}_2$  is more reactive. If we start with surface H from  $\text{NH}_2$  for the hydrogen transfer step, the relaxed structure shows that the surface N atom grabs the H atom from channel N atom and recover to  $\text{NH}_2$ , and the channel N atom migrates to surface site. Due to the strong adsorption strength, the resulting hydrogen transfer step is highly endothermic with a positive energy difference of  $1.41\text{eV}$  and a very high computed activation barrier of  $2.01\text{eV}$ .

After the first Cp ligand desorption, another channel NH will migrate to surface site to be ready to react with the second Cp ligand. The second hydrogen transfer reaction is less endothermic with slightly positive reaction energy difference of  $0.46\text{eV}$  and lower barrier with the value of  $1.00\text{eV}$ . Finally, after the second Cp ligand desorption, the reaction energy is still negative ( $-1.53\text{eV}$ ). This implies that upon adsorption of  $\text{RuCp}_2$  on Ru(100) at  $0.67\text{ML NH}$  and  $0.67\text{ML NH}_2$  terminations, two hydrogen transfer steps can take place, although this will be limited by the barrier for H transfer as a result of the extremely stable adsorption mode of the  $\text{RuCp}_2$  precursor.

On Co(100) surface, the reaction energies for all steps are negative so that the overall reaction loss of two Cp ligands as  $\text{CpH}$  is exothermic by  $-0.79\text{eV}$ . The  $\text{CoCp}_2$  precursor has a strong initial adsorption mode on Co(100) surface, which is  $-1.67\text{eV}$ . The hydrogen transfer step is exothermic,

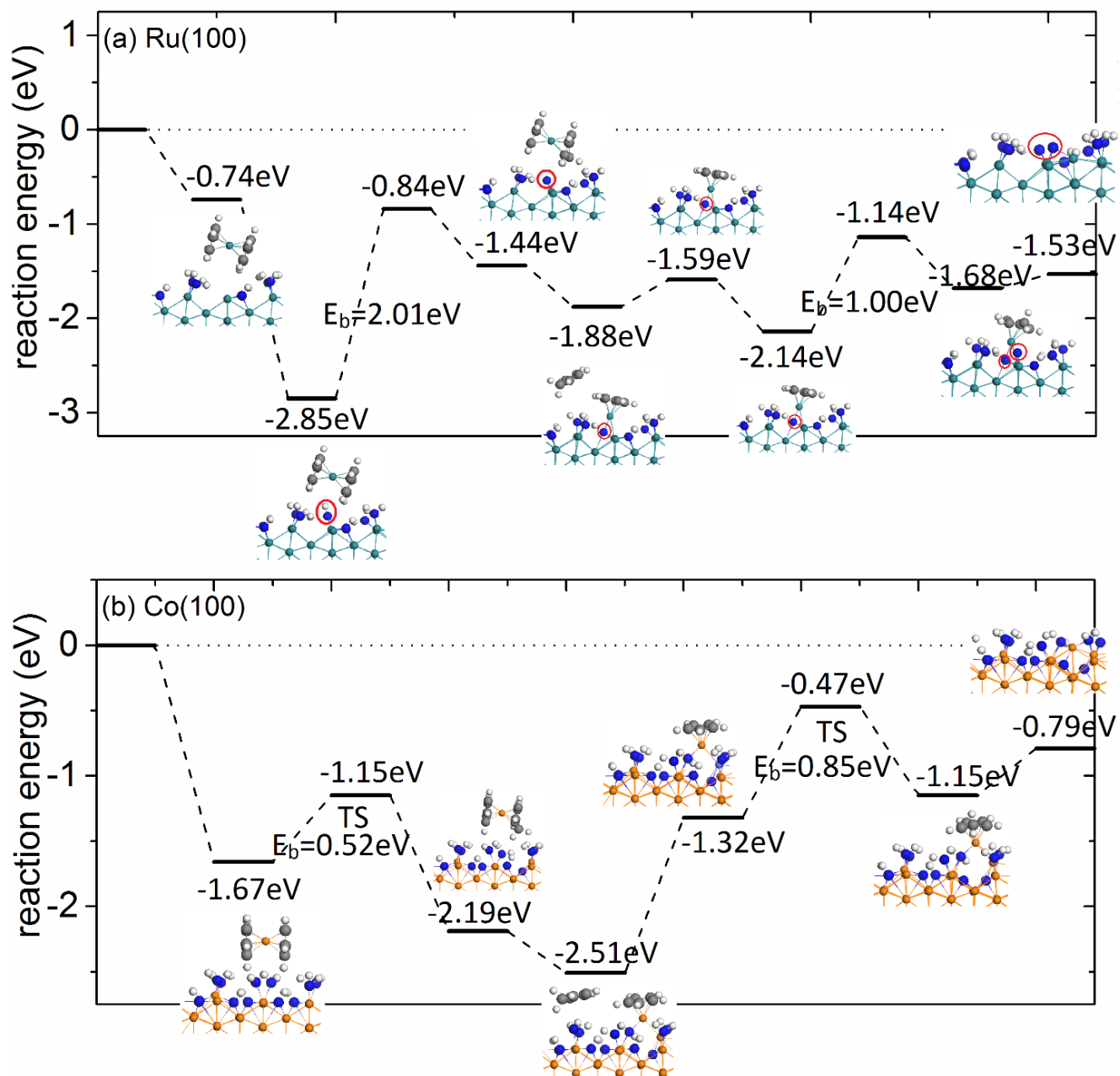


Figure 8. The plotted metal precursor reaction pathway on (a) Ru(100) surface and (b) Co(100) surface at ALD operating condition. On both Ru(100) and Co(100) surfaces, the two Cp ligands can be eliminated with Ru or Co atom deposited on the surface.

with a computed energy change of  $-0.52\text{eV}$  and a moderate barrier of  $0.52\text{eV}$ . After the first Cp ligand desorption, the second hydrogen transfer step is practically thermoneutral with a small endothermic energy difference of  $0.17\text{eV}$  and a moderate barrier of  $0.85\text{eV}$ . Finally, the desorption of the second Cp ligand shows an energy gain of  $-0.79\text{eV}$  and the resulting structure is Co atom binding to N atom that has lost H atom.

To summarize, for  $\text{NH}_x$  terminations of Ru and Co at typical ALD operating condition, on both Ru and Co (001) surface, the second Cp ligand elimination is impossible and the termination is most likely to be  $\text{MCp}$  ( $\text{M}=\text{Ru}, \text{Co}$ ) fragments. The desorption of  $\text{CpH}$  on Ru and Co (001) surface is endothermic but this can be achieved at ALD operating temperature. On the (100) surfaces, both  $\text{RuCp}_2$  and  $\text{CoCp}_2$  can undergo two hydrogen transfer step and Cp ligand elimination reactions. However,  $\text{RuCp}_2$  has much higher barrier than  $\text{CoCp}_2$  for the hydrogen transfer step. Thus, final termination on Ru(100) surface could be strongly adsorbed  $\text{RuCp}_2$  metal precursors. The final structures after single metal precursor  $\text{MCp}_2$  ( $\text{M}=\text{Ru}$  or  $\text{Co}$ ) adsorbing and reacting on  $\text{NH}_x$ -terminated metal (100) surfaces are shown in Figure 9.

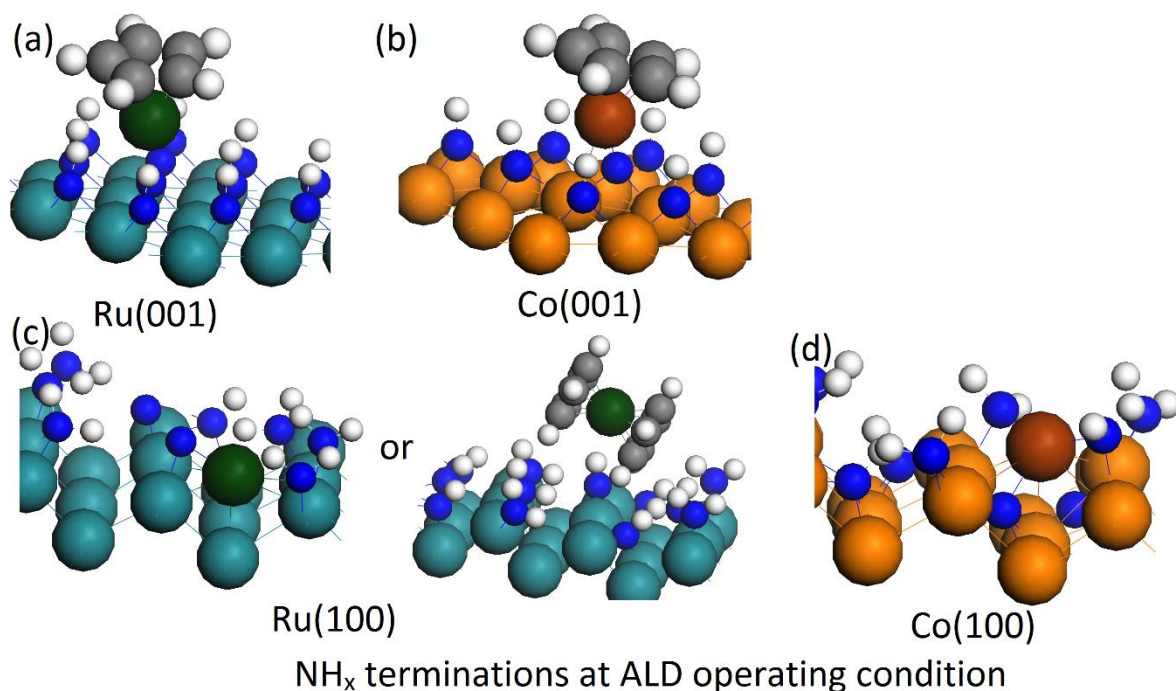


Figure 9. The configurations of the final structures after single metal precursor MCP<sub>2</sub> (M=Ru or Co) adsorption and ligand elimination on the (a) Ru(001), (b) Co(001), (c) Ru(100), and (d) Co(100) surface. The NH<sub>x</sub> terminations are at ALD operating condition.

#### 4. Conclusions

When depositing metals, a non-oxidizing reactant is preferred because the O-source will cause contamination and oxidize metals. The ALD of Ru and Co using metal precursor and N-plasma have been investigated experimentally but the reaction mechanism is not well-understood. After the N-plasma step, the resulted metal surfaces will be NH<sub>x</sub>-terminated. The nature and stability of NH<sub>x</sub>-terminated metal surfaces are studied in our previous published work.<sup>48</sup> The present work focuses on the reaction mechanism during the metal precursor pulse at the NH<sub>x</sub>-terminated surfaces. The surface facets will result in different precursor adsorption orientation. RuCp<sub>2</sub> and

CoCp<sub>2</sub> prefer up-right position with one Cp ring in close contact with NH<sub>x</sub>-terminated (001) surface, while they are in flat position with both of the Cp rings anchored to zigzag channel on NH<sub>x</sub>-terminated (100) surface.

The Cp ligands can be eliminated via hydrogen transfer step and desorb from surface by forming CpH. The NH<sub>x</sub>-termination is determined at both zero-K condition and ALD operating condition.<sup>48</sup>

The NH<sub>x</sub>-termination plays an important role in reaction energy and barriers for hydrogen transfer step, with the exception of the Ru(001). 1ML NH is preferred on Ru(001) surface at zero-K. With increasing temperature, NH will gradually desorb from surface, resulting in 0.89ML NH at ALD operating condition. However, the hydrogen transfer reaction on Ru(001) surface is endothermic and the barrier is as high as 1.33eV and 1.51eV for 1ML NH termination and 0.89ML NH termination. Continuing decreasing NH coverage to extremely condition with 0.06ML NH (one NH on (4×4) supercell) leads to the similar positive reaction energy difference and high barrier. The hydrogen transfer step on Ru(001) surface is thermodynamically and kinetically unfavourable.

On the Co(001) surface, 0.67ML NH and 0.23ML NH<sub>2</sub> is the preferred termination at zero-K and the coverage is 0.56ML NH at ALD operating condition. CoCp<sub>2</sub> can perform two hydrogen transfer steps and results in a Co atom deposited on the surface for 0.67ML NH and 0.23ML NH<sub>2</sub> termination; while only one Cp ligand can be eliminated at the lower coverage of 0.56ML NH terminated Co(001) surface. For the terminations at zero-K condition, there is NH<sub>3</sub> formation. Surface terminating N and H species may be eliminated via NH<sub>3</sub> formation during the metal precursor step as well as during the next plasma step to deposit metal atom onto the surface.

On the (100) surface, 1ML NH and 1ML NH<sub>2</sub> is the preferred termination at zero-K condition and this coverage is reduced to 0.67ML NH and 0.67ML NH<sub>2</sub> at ALD operating condition. The reactivity is greatly improved compared to the Ru(100) surface at zero-K condition. At full

coverage, only one Cp ligand can be eliminated, while at 0.67ML NH and 0.67ML NH<sub>2</sub> termination, the final structure is Ru atom deposited on the surface with two Cp ligands elimination, although this has very high barriers. On the Co(100) surface, although the final structure is Co atom deposition on the surface for both terminations, the termination at ALD operating condition has a lower barrier than the termination at zero-K condition. For the hydrogen transfer step, CoCp<sub>2</sub> always has lower reaction barriers than RuCp<sub>2</sub>, regardless of surface facets or NH<sub>x</sub> coverage.

Thus, after metal precursor pulse, at ALD operating condition, the (001) surface will be terminated with RuCp or CoCp fragments binding to N atom and unreacted NH<sub>x</sub> species; while (100) surface is terminated with Ru or Co atom binding to N atom and unreacted NH<sub>x</sub> species. During the plasma step, the remaining Cp ligand (if any) and surface N atom are eliminated by N<sub>x</sub>H<sub>y</sub> radicals from the N-plasma (NH<sub>3</sub> or mixture of N<sub>2</sub> and H<sub>2</sub>). After the plasma pulse, the metal surface will be NH<sub>x</sub>-terminated and the while system is ready for the next cycle. The reaction mechanism of N-plasma step is currently the subject of further study.

## References

1. Tu, K., Recent advances on electromigration in very-large-scale-integration of interconnects. *J. Appl. Phys.* **2003**, 5451-5473.
2. Greenslit, D. V.; Eisenbraun, E., Characterization of Ultrathin PEALD-Grown RuCo Films for Diffusion Barrier and Copper Direct-Plate Applications. *ECS Trans.* **2011**, *35*, 17-24.
3. Chakraborty, T.; Eisenbraun, E. T., Microstructure analysis of plasma enhanced atomic layer deposition-grown mixed-phase RuTaN barrier for seedless copper electrodeposition. *J. Vac. Sci. Technol. A* **2012**, *30*, 020604.
4. Miikkulainen, V.; Leskelä, M.; Ritala, M.; Puurunen, R. L., Crystallinity of inorganic films grown by atomic layer deposition: Overview and general trends. *J. Appl. Phys.* **2013**, *113*, 2.
5. Johnson, R. W.; Hultqvist, A.; Bent, S. F., A brief review of atomic layer deposition: from fundamentals to applications. *Mater. Today* **2014**, *17*, 236-246.
6. Kaloyeros, A. E.; Pan, Y.; Goff, J.; Arkles, B., Review—Cobalt Thin Films: Trends in Processing Technologies and Emerging Applications. *ECS J. Solid State Sci.* **2019**, *8*, P119-P152.
7. Mallick, B. C.; Hsieh, C. T.; Yin, K. M.; Gandomi, Y. A.; Huang, K. T., Review-On Atomic Layer Deposition: Current Progress and Future Challenges. *Ecs J Solid State Sc* **2019**, *8*, N55-N78.
8. George, S. M., Atomic layer deposition: an overview. *Chem. Rev.* **2009**, *110*, 111-131.
9. Profijt, H.; Potts, S.; Van de Sanden, M.; Kessels, W., Plasma-assisted atomic layer deposition: basics, opportunities, and challenges. *J. Vac. Sci. Technol. A* **2011**, *29*, 050801.
10. Oviroh, P. O.; Akbarzadeh, R.; Pan, D.; Coetzee, R. A. M.; Jen, T. C., New development of atomic layer deposition: processes, methods and applications. *Sci. Technol. Adv. Mater.* **2019**, *20*, 465-496.
11. Kim, H., Atomic layer deposition of metal and nitride thin films: Current research efforts and applications for semiconductor device processing. *J. Vac. Sci. Technol. B* **2003**, *21*, 2231-2261.
12. Ramos, K. B.; Saly, M. J.; Chabal, Y. J., Precursor design and reaction mechanisms for the atomic layer deposition of metal films. *Coordin. Chem. Rev.* **2013**, *257*, 3271-3281.
13. Aaltonen, T.; Alén, P.; Ritala, M.; Leskelä, M., Ruthenium thin films grown by atomic layer deposition. *Chem. Vap. Depos.* **2003**, *9*, 45-49.
14. Hämäläinen, J.; Ritala, M.; Leskelä, M., Atomic Layer Deposition of Noble Metals and Their Oxides. *Chem. Mater.* **2014**, *26*, 786-801.
15. Park, S.-J.; Kim, W.-H.; Maeng, W.; Yang, Y.; Park, C.; Kim, H.; Lee, K.-N.; Jung, S.-W.; Seong, W., Effect oxygen exposure on the quality of atomic layer deposition of ruthenium from bis (cyclopentadienyl) ruthenium and oxygen. *Thin Solid Films* **2008**, *516*, 7345-7349.

16. Leick, N.; Verkuijlen, R.; Lamagna, L.; Langereis, E.; Rushworth, S.; Roozeboom, F.; Van de Sanden, M.; Kessels, W., Atomic layer deposition of Ru from CpRu (CO) <sub>2</sub> Et using O <sub>2</sub> gas and O <sub>2</sub> plasma. *J. Vac. Sci. Technol. A* **2011**, *29*, 021016.
17. Lee, S.-J.; Kim, S.-H., Effects of Annealing on the Properties of Atomic Layer Deposited Ru Thin Films Deposited by NH<sub>3</sub> and H<sub>2</sub> as Reactants. *Thin Solid Films* **2016**, *612*, 122-127.
18. Lee, S.-J.; Kim, S.-H.; Saito, M.; Suzuki, K.; Nabeya, S.; Lee, J.; Kim, S.; Yeom, S.; Lee, D.-J., Plasma-Free Atomic Layer Deposition of Ru Thin Films Using H<sub>2</sub> Molecules as A Nonoxidizing Reactant. *J. Vac. Sci. Technol. A* **2016**, *34*, 031509.
19. Gakis, G. P.; Vergnes, H.; Cristiano, F.; Tison, Y.; Vahlas, C.; Caussat, B.; Boudouvis, A. G.; Scheid, E., In situ N<sub>2</sub>-NH<sub>3</sub> plasma pre-treatment of silicon substrate enhances the initial growth and restricts the substrate oxidation during alumina ALD. *J. Appl. Phys* **2019**, *126*, 125305.
20. Swerts, J.; Delabie, A.; Salimullah, M.; Popovici, M.; Kim, M.-S.; Schaeckers, M.; Van Elshocht, S., Impact of the plasma ambient and the ruthenium precursor on the growth of ruthenium films by plasma enhanced atomic layer deposition. *Electrochem. Solid-State Lett.* **2012**, *1*, P19-P21.
21. Park, S.-J.; Kim, W.-H.; Maeng, W.; Kim, H., Thermal and plasma enhanced atomic layer deposition ruthenium and electrical characterization as a metal electrode. *Microelectron. Eng.* **2008**, *85*, 39-44.
22. Knisley, T. J.; Kalutarage, L. C.; Winter, C. H., Precursors and chemistry for the atomic layer deposition of metallic first row transition metal films. *Coordin. Chem. Rev.* **2013**, *257*, 3222-3231.
23. Kim, H., Area selective atomic layer deposition of cobalt thin films. *ECS Trans.* **2008**, *16*, 219-225.
24. Lim, B. S.; Rahtu, A.; Gordon, R. G., Atomic layer deposition of transition metals. *Nat. Mater.* **2003**, *2*, 749.
25. Kim, H., High-quality cobalt thin films by plasma-enhanced atomic layer deposition. *Electrochem. Solid-State Lett.* **2006**, *9*, G323-G325.
26. Kim, K.; Lee, K.; Han, S.; Jeong, W.; Jeon, H., Characteristics of cobalt thin films deposited by remote plasma ALD method with dicobalt octacarbonyl. *J. Electrochem. Soc.* **2007**, *154*, H177-H181.
27. Zhu, B.; Ding, Z.-J.; Wu, X.; Liu, W.-J.; Zhang, D. W.; Ding, S.-J., Plasma-Enhanced Atomic Layer Deposition of Cobalt Films Using Co (EtCp) <sub>2</sub> as a Metal Precursor. *Nanoscale Res. Lett.* **2019**, *14*, 76.
28. Yoon, J.; Kim, D.; Cheon, T.; Kim, S.-H.; Kim, H., Atomic layer deposition of Co using N<sub>2</sub>/H<sub>2</sub> plasma as a reactant. *J. Electrochem. Soc.* **2011**, *158*, H1179-H1182.

29. Vos, M. F.; van Straaten, G.; Kessels, W. E.; Mackus, A. J., Atomic Layer Deposition of Cobalt Using H<sub>2</sub>-, N<sub>2</sub>-, and NH<sub>3</sub>-Based Plasmas: On the Role of the Co-reactant. *J. Phys. Chem. C* **2018**, *122*, 22519-22529.
30. Elliott, S. D., Atomic-scale simulation of ALD chemistry. *Semicond. Sci. Tech.* **2012**, *27*, 074008.
31. Phung, Q. M.; Pourtois, G.; Swerts, J.; Pierloot, K.; Delabie, A., Atomic Layer Deposition of Ruthenium on Ruthenium Surfaces: A Theoretical Study. *J. Phys. Chem. C* **2015**, *119*, 6592-6603.
32. Elliott, S. D.; Dey, G.; Maimaiti, Y., Classification of processes for the atomic layer deposition of metals based on mechanistic information from density functional theory calculations. *J. Chem. Phys.* **2017**, *146*, 052822.
33. Phung, Q. M.; Vancoillie, S.; Pourtois, G.; Swerts, J.; Pierloot, K.; Delabie, A., Atomic Layer Deposition of Ruthenium on a Titanium Nitride Surface: A Density Functional Theory Study. *J. Phys. Chem. C* **2013**, *117*, 19442-19453.
34. Fang, G.; Xu, L.; Cao, Y.; Li, A., Theoretical design and computational screening of precursors for atomic layer deposition. *Coordin. Chem. Rev.* **2016**, *322*, 94-103.
35. Holme, T. P.; Prinz, F. B., Atomic Layer Deposition and Chemical Vapor Deposition Precursor Selection Method Application to Strontium and Barium Precursors. *J. Phys. Chem. A* **2007**, *111*, 8147-8151.
36. Puurunen, R. L., Surface chemistry of atomic layer deposition: A case study for the trimethylaluminum/water process. *J. Appl. Phys.* **2005**, *97*, 9.
37. Elliott, S.; Scarel, G.; Wiemer, C.; Fanciulli, M.; Pavia, G., Ozone-Based Atomic Layer Deposition of Alumina from TMA: Growth, Morphology, and Reaction Mechanism. *Chem. Mater.* **2006**, *18*, 3764-3773.
38. Langereis, E.; Bouman, M.; Keijmel, J.; Heil, S.; Van de Sanden, M.; Kessels, W., Plasma-assisted ALD of Al<sub>2</sub>O<sub>3</sub> at low temperatures: reaction mechanisms and material properties. *ECS Trans.* **2008**, *16*, 247-255.
39. Rai, V. R.; Vandalon, V.; Agarwal, S., Surface reaction mechanisms during ozone and oxygen plasma assisted atomic layer deposition of aluminum oxide. *Langmuir* **2010**, *26*, 13732-13735.
40. Weckman, T.; Laasonen, K., First principles study of the atomic layer deposition of alumina by TMA-H<sub>2</sub>O-process. *Phys. Chem. Chem. Phys.* **2015**, *17*, 17322-17334.
41. Elam, J.; Pellin, M.; Elliott, S. D.; Zydor, A.; Faia, M.; Hupp, J. T., Mechanism for zirconium oxide atomic layer deposition using bis (methylcyclopentadienyl) methoxymethyl zirconium. *Appl. Phys. Lett.* **2007**, *91*, 253123.
42. Nolan, M.; Elliott, S. D., Competing mechanisms in atomic layer deposition of Er<sub>2</sub>O<sub>3</sub> versus La<sub>2</sub>O<sub>3</sub> from cyclopentadienyl precursors. *Chem. Mater.* **2009**, *22*, 117-129.

43. Zydor, A.; Elliott, S. D., Thermal Stability of Precursors for Atomic Layer Deposition of TiO<sub>2</sub>, ZrO<sub>2</sub>, and HfO<sub>2</sub>: An Ab Initio Study of  $\alpha$ -Hydrogen Abstraction in Bis-Cyclopentadienyl Dimethyl Complexes. *J. Phys. Chem. A* **2010**, *114*, 1879-1886.
44. Tanskanen, J. T.; Hägglund, C.; Bent, S. F., Correlating Growth Characteristics in Atomic Layer Deposition with Precursor Molecular Structure: The Case of Zinc Tin Oxide. *Chem. Mater.* **2014**, *26*, 2795-2802.
45. Weckman, T.; Laasonen, K., Atomic Layer Deposition of Zinc Oxide: Diethyl Zinc Reactions and Surface Saturation from First-Principles. *J. Phys. Chem. C* **2016**, *120*, 21460-21471.
46. Weckman, T.; Laasonen, K., Atomic Layer Deposition of Zinc Oxide: Study on the Water Pulse Reactions from First-Principles. *J. Phys. Chem. C* **2018**, *122*, 7685-7694.
47. Elliott, S. D., Mechanism, Products, and Growth Rate of Atomic Layer Deposition of Noble Metals. *Langmuir* **2010**, *26*, 9179-9182.
48. Liu, J.; Nolan, M., Coverage and Stability of NH<sub>x</sub>-Terminated Cobalt and Ruthenium Surfaces: A First-Principles Investigation. *J. Phys. Chem. C* **2019**, *123*, 25166-25175.
49. Kresse, G.; Joubert, D., From ultrasoft pseudopotentials to the projector augmented-wave method. *Phys. Rev. B* **1999**, *59*, 1758.
50. Perdew, J. P.; Chevary, J. A.; Vosko, S. H.; Jackson, K. A.; Pederson, M. R.; Singh, D. J.; Fiolhais, C., Atoms, molecules, solids, and surfaces: Applications of the generalized gradient approximation for exchange and correlation. *Phys. Rev. B* **1992**, *46*, 6671.
51. Perdew, J. P.; Burke, K.; Ernzerhof, M., Generalized gradient approximation made simple. *Phys. Rev. Lett.* **1996**, *77*, 3865.
52. Monkhorst, H. J.; Pack, J. D., Special points for Brillouin-zone integrations. *Phys. Rev. B* **1976**, *13*, 5188.
53. Maimaiti, Y.; Elliott, S. D., Precursor Adsorption on Copper Surfaces as the First Step during the Deposition of Copper: A Density Functional Study with van der Waals Correction. *J. Phys. Chem. C* **2015**, *119*, 9375-9385.
54. Henkelman, G.; Uberuaga, B. P.; Jónsson, H., A climbing image nudged elastic band method for finding saddle points and minimum energy paths. *J. Chem. Phys.* **2000**, *113*, 9901-9904.

# Graphic abstract

